29. G. Chang, R. Spencer, A. Lee, M. Barclay, D. Rees, data not shown.
30. A. Kreusch, P. J. Pfaffinger, C. F. Stevens, S. Choe, *Nature* **392**, 945 (1998).
31. X. R. Ou, P. Blount, R. J. Hoffman, C. Kung, *Proc. Natl. Acad. Sci. U.S.A.* **95**, 11471 (1998).
32. P. Blount, S. I. Sukharev, M. J. Schroeder, S. K. Nagle, C. Kung, *ibid.* **93**, 11652 (1996).
33. C. C. Hase, A. C. LeDain, B. Martinac, *J. Membr. Biol.* **157**, 17 (1997).
34. ———, *J. Biol. Chem.* **270**, 18329 (1995).
35. W. J. Sigurdson, S. I. Sukharev, C. Kung, F. Sachs, *Biophys. J.* **72**, WP104 (1997).
36. H. A. Lester, *Annu. Rev. Biophys. Biomol. Struct.* **21**, 267 (1992).
37. N. Unwin, *Nature* **373**, 37 (1995).
38. ———, *J. Mol. Biol.* **257**, 586 (1996).
39. S. Bailey, CCP4 Project, *Acta Crystallogr. D* **50**, 760 (1994).
40. Single-letter abbreviations for the amino acid residues are as follows: A, Ala; C, Cys; D, Asp; E, Glu; F, Phe; G, Gly; H, His; I, Ile; K, Lys; L, Leu; M, Met; N, Asn; P, Pro; Q, Gln; R, Arg; S, Ser; T, Thr; V, Val; W, Trp; and Y, Tyr.
41. J. D. Thompson, T. J. Gibson, F. Plewniak, F. Jeanmougin, D. G. Higgins, *Nucleic Acids Res.* **25**, 4876 (1997).
42. R. M. Esnouf, *J. Mol. Graphics* **15**, 132 (1997).
43. P. J. Kraulis, *J. Appl. Crystallogr.* **24**, 946 (1991).
44. E. A. Merritt and D. J. Bacon, *Methods Enzymol.* **277**, 505 (1997).
45. B. Honig and A. Nicholls, *Science* **268**, 1144 (1995).
46. We thank A. Chirino for advice and computer support, J. G. Spencer for technical assistance, S. Gordon of the Institut Pasteur (Paris, France) for his kind gift of genomic DNA from *M. tuberculosis*, C. Kung and P. C. Moe from the University of Wisconsin–Madison for several cloned *mscL* homologs and for the *E. coli* knockout mutant for *mscL*, A. Okabe of the Kagawa Medical School (Kagawa, Japan) for providing cloned DNA of *mscL* from *C. perfringens*, and D. Dougherty and H. Lester for helpful discussions. We also thank the staff at the Stanford Synchrotron Radiation Laboratory (SSRL) and the Advanced Light Source (ALS) for their help in data collection. The synchrotron rotation camera facilities are supported by the U.S. Department of Energy (ALS and SSRL) and NIH (SSRL). G.C. and R.H.S. were supported by NIH postdoctoral fellowship grant GM18486 and an Amgen postdoctoral fellowship, respectively, during the initial stages of this project. Supported by the Howard Hughes Medical Institute. Protein Data Bank identifier for Tb-MscL is 1MSL.

29 October 1998; accepted 16 November 1998

Regulation of Polar Auxin Transport by AtPIN1 in *Arabidopsis* Vascular Tissue

Leo Gälweiler, Changhui Guan, Andreas Müller, Ellen Wisman, Kurt Mendgen, Alexander Yephremov, Klaus Palme*

Polar auxin transport controls multiple developmental processes in plants, including the formation of vascular tissue. Mutations affecting the *PIN-FORMED (PIN1)* gene diminish polar auxin transport in *Arabidopsis thaliana* inflorescence axes. The *AtPIN1* gene was found to encode a 67-kilodalton protein with similarity to bacterial and eukaryotic carrier proteins, and the AtPIN1 protein was detected at the basal end of auxin transport–competent cells in vascular tissue. AtPIN1 may act as a transmembrane component of the auxin efflux carrier.

Charles Darwin had proposed the concept of translocated chemical messengers in higher plants, which finally resulted in the discovery of polar auxin transport in the 1930s (*1*). The transport of auxin from the plant tip downward provides directional information, influencing vascular tissue differentiation, apical development, organ regeneration, tropic growth, and cell elongation (*2*, *3*). Polar auxin transport can be monitored by following the movement of radiolabeled auxin through tissues. Auxin transport is specific for the major auxin indoleacetic acid and various synthetic auxins, it requires energy, and it occurs with a velocity of 7 to 15 mm/hour (*2*). This transport can be specifically inhibited by synthetic compounds, known as polar auxin transport inhibitors, and by naturally occurring flavonoids (*4*). The current concept, known as the "chemiosmotic hypothesis," proposes that (i) the driving force for polar auxin transport is provided by the transmembrane proton motive force, and that (ii) the cellular efflux of auxin anions is mediated by saturable, auxin-specific carriers in shoots presumably located at the basal end of transport-competent cells (*2*). Immunocytochemical work with monoclonal antibodies to pea stem cell fractions indicated that the auxin efflux carrier is located at the basal end of auxin transport–competent cells (*5*).

Gene tagging. The phenotype of the *pin-formed* mutant of *Arabidopsis* can be mimicked by chemical inhibition of polar auxin transport (*6*). Analysis of auxin transport in *pin-formed* mutants suggests that an essential component for auxin transport is affected (*6*, *7*). To isolate the affected *AtPIN1* gene locus, we used the autonomous transposable element *En-1* from maize to generate mutants in *Arabidopsis thaliana*. We identified three independent transposon-induced mutants, *Atpin1::En134*, *Atpin1::En111*, and *Atpin1::En349*, that exhibited auxin transport–deficient phenotypes (*8*). These plants developed naked, pin-shaped inflorescences

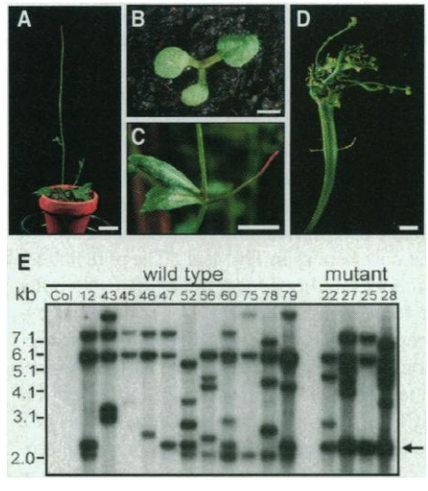

Fig. 1. Phenotypic and Southern blot analysis of the transposon insertional mutant *Atpin1::En134*. (**A**) The most obvious phenotypic aspect of the homozygous mutant represents the naked, pin-forming inflorescence with no or just a few defective flowers. (**B**) *Atpin1::En134* seedlings showed frequently aberrant cotyledon positioning or triple cotyledons. (**C**) A mutant cauline leaf exhibited abnormal vein branching resulting in the appearance of fused twin or triple leaves. Unusually, the leaf and "pin"-forming axillary shoot have formed in opposite positions. (**D**) Drastically fasciated inflorescence of an aged mutant. (**E**) Southern blot analysis of a segregating *Atpin1::En134* mutant population. The M_2 progeny of the heterozygous *Atpin1::En134* mutant showed 3:1 segregation for wild-type and mutant phenotype plants (*8*). The cetyltrimethylammonium bromide method (*23*) was used to isolate genomic DNA from plants showing the mutant (22, 27, 25 28) and wild-type (12, 43, 45, 46, 47, 52, 56, 60, 75, 78, 79) phenotype and from ecotype Columbia (Col) plants lacking *En-1* insertions. After Xba I digestion, the DNA was separated on a 0.8% agarose gel (2 μg per lane), transferred to a Nylon membrane and hybridized with a ^{32}P-labeled 3′-end probe of the *En-1* transposon (*24*). Only one fragment of 2.3 kb in length (marked by an arrow) was commonly detected in all 12 tested homozygous *Atpin1::En134* mutants and in 15 heterozygous plants (not all are shown), indicating cosegregation with the *Atpin1::En134* allele. Size bars represent 25 mm (A), 2.5 mm (B), and 10 mm [(C) and (D)].

L. Gälweiler, C. Guan, A. Müller, and K. Palme are at the Max-Delbrück-Laboratorium in der Max-Planck-Gesellschaft, Carl-von-Linné-Weg 10, D-50829 Köln, Germany. E. Wisman and A. Yephremov are at the Max-Planck-Institut für Züchtungsforschung, Abteilung Molekulare Pflanzengenetik, Carl-von-Linné-Weg 10, D-50829 Köln, Germany. K. Mendgen is at the Universität Konstanz, Fakultät für Biologie/Phytopathologie, D-78457 Konstanz, Germany.

*To whom correspondence should be addressed. E-mail: palme@mpiz-koeln.mpg.de

and abnormalities in the number, size, shape, and position of lateral organs (Fig. 1, A to D), similar to those described for the *pin-formed* mutant (*6, 7*). In crosses between heterozygous *pin-formed* and *Atpin1::En134* mutants, 25% of the F_1 progeny showed the mutant phenotype, indicating that these mutations were alleles of the same gene (*9*). Further analysis showed that *Atpin1::En111* and *Atpin1::En349* were also allelic to *Atpin1::En134* (Fig. 2A) (*10*).

The *AtPIN1* gene. To identify the *En-1* transposon insertion responsible for the mutant phenotype, we performed Southern (DNA) blot analysis with the M_2 progeny of a heterozygous *Atpin1::En134* mutant. An *En-1* probe corresponding to the 3′ end of the transposon detected a single 2.3-kb fragment of Xba I–digested genomic DNA cosegregating with plants showing the mutant phenotype. This fragment was also detected in heterozygous plants, which segregated the mutant phenotype in about 25% of their M_3 progeny, as expected for a recessive mutation (Fig. 1E). DNA flanking the tagged locus was isolated from the genomic DNA of homozygous *Atpin1::En134* mutant plants with the use of a ligation-mediated polymerase chain reaction (PCR). The resulting PCR fragment was sequenced and used as a probe to isolate homologous clones from wild-type *Arabidopsis* genomic and complementary DNA (cDNA) libraries (*11*). DNA sequence analysis revealed that the *AtPIN1* gene consisted of five exons with lengths of 1246, 235, 244, 77, and 64 nucleotides (Fig. 2A). Analysis of mutant *Atpin1* transposon insertional alleles showed that the *En-1* element was inserted into the first exon of the *AtPIN1* gene (Fig. 2A). Excision of the *En-1* transposon from the *Atpin1::En134* and *Atpin1::En349* alleles resulted in revertant alleles that restored the wild-type phenotype. Sequence analysis of the revertant alleles confirmed that the *En-1* element had excised from the first *AtPIN1* exon, resulting in an exact restoration of the *AtPIN1* open reading frame (*9*).

Northern (RNA) blot hybridizations with an *AtPIN1*-specific probe showed that the gene was transcribed in all wild-type organs tested, yielding a transcript signal of 2.3 kb in length (Fig. 3A). *AtPIN1* gene expression was absent in the homozygous transposon insertional mutants *Atpin1::En134* (Fig. 3B, lane 2) and *Atpin1::En349* (Fig. 3B, lane 5). Heterozygous plants (Fig. 3B, lanes 1, 4, and 6) showed *AtPIN1* expression, probably from their wild-type allele. Similarly, homozygous *pin-formed* mutants did not express *AtPIN1* (Fig. 3A, lane 3). We used an *AtPIN1* cDNA probe to identify a yeast artificial chromosome (YAC) contig from the CIC YAC library that represented a region between centimorgan 92.7 and 113.6 in chromosome 1 of *Arabidopsis* similar to the location of the *PIN-FORMED* locus (*7, 12*). These data from genetic analysis, physical mapping, and gene

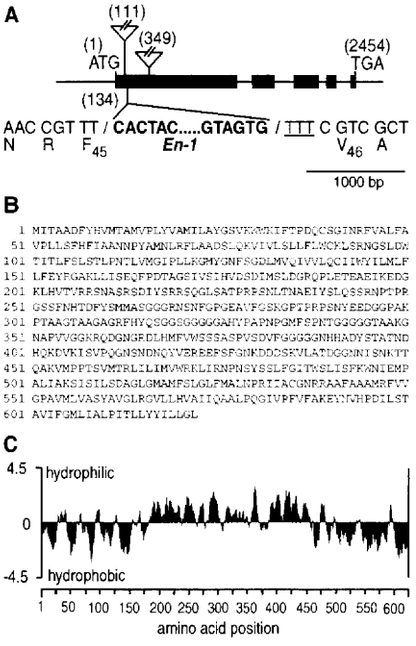

Fig. 2. Structural analysis of *AtPIN1* alleles and of the deduced AtPIN1 amino acid sequence. (**A**) Structure of the *AtPIN1* gene (drawn to scale), with black boxes representing exons and mapped *En-1* insertion sites in the independent mutant alleles *Atpin1::En111* (111), *Atpin1::En134* (134), and *Atpin1::En349* (349). Numbers in brackets show base pair positions. The positions of the translational start (ATG) and termination codons (TGA) of the predicted open reading frame are depicted. Nucleotide sequences flanking both ends of the *En-1* transposon in *Atpin1::En134* show the disruption of the coding sequence at codon 45 (F). The duplication of nucleotide triplets (TTT) is characteristic for *En-1* insertion sites (*25*). (**B**) Amino acid sequence (*26*) deduced from the *AtPIN1* cDNA (accession number AF089084). (**C**) Hydropathy analysis of AtPIN1. The hydropathy plot was generated with the Lasergene software (DNAstar, Madison, Wisconsin) and the method of Kyte and Doolittle with a window size of nine amino acids (*27*).

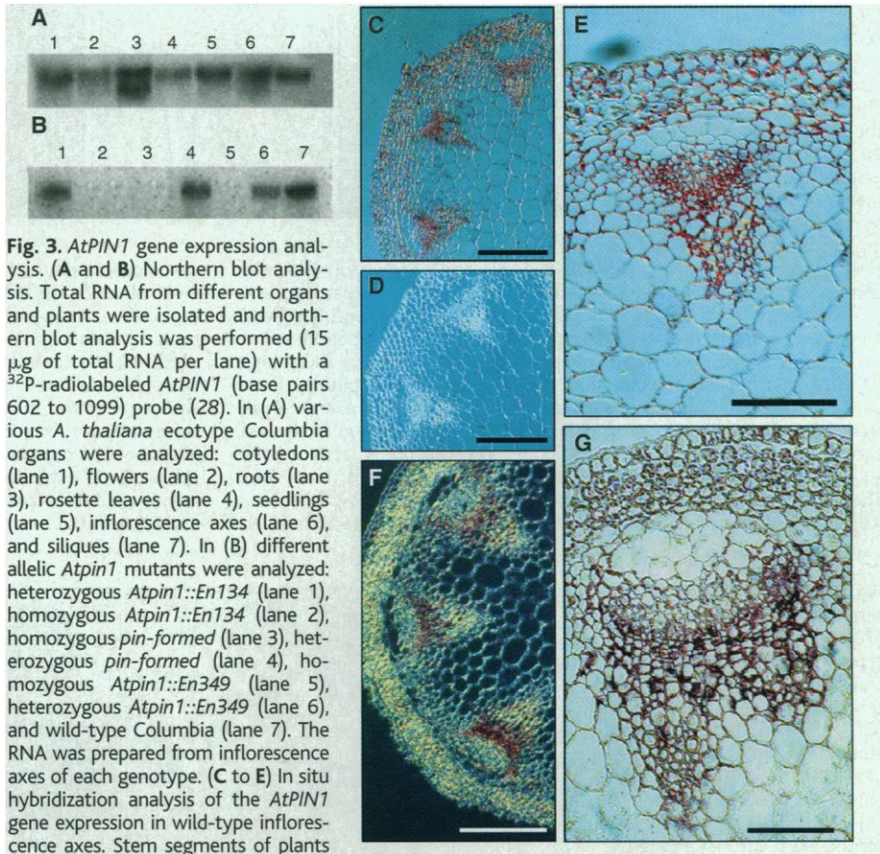

Fig. 3. *AtPIN1* gene expression analysis. (**A** and **B**) Northern blot analysis. Total RNA from different organs and plants were isolated and northern blot analysis was performed (15 μg of total RNA per lane) with a ^{32}P-radiolabeled *AtPIN1* (base pairs 602 to 1099) probe (*28*). In (A) various *A. thaliana* ecotype Columbia organs were analyzed: cotyledons (lane 1), flowers (lane 2), roots (lane 3), rosette leaves (lane 4), seedlings (lane 5), inflorescence axes (lane 6), and siliques (lane 7). In (B) different allelic *Atpin1* mutants were analyzed: heterozygous *Atpin1::En134* (lane 1), homozygous *Atpin1::En134* (lane 2), homozygous *pin-formed* (lane 3), heterozygous *pin-formed* (lane 4), homozygous *Atpin1::En349* (lane 5), heterozygous *Atpin1::En349* (lane 6), and wild-type Columbia (lane 7). The RNA was prepared from inflorescence axes of each genotype. (**C** to **E**) In situ hybridization analysis of the *AtPIN1* gene expression in wild-type inflorescence axes. Stem segments of plants were fixed, paraffin embedded, cross sectioned (8 μm), and probed with either antisense [(C) and (E)] or sense (D), digoxigenin-labeled, in vitro–transcribed *AtPIN1* RNA. The *AtPIN1* transcript signals were indirectly visualized with the help of alkaline phosphatase–conjugated secondary antibodies (*29*). (E) is a magnified section of a vascular bundle of (C). *AtPIN1*-specific staining (red) is localized in cambial and xylem tissues. (**F** and **G**) Immunocytochemical localization of AtPIN1 protein in cross sections of inflorescence axes. Stem segments of wild-type plants were fixed, paraffin embedded, sectioned (8 μm), and incubated with affinity-purified polyclonal anti-AtPIN1. Bound anti-AtPIN1 was visualized with the help of alkaline phosphatase–conjugated secondary antibodies (*18, 30*). AtPIN1-specific staining (purple) was found in cambial and in young and parenchymatous xylem cells (G). Size bars represent 100 μm [(E) and (G)] and 200 μm [(C), (D), and (F)].

expression studies confirmed that the cloned *AtPIN1* gene corresponded to the *PIN-FORMED* locus. As the phenotypes of both *pin-formed* and *Atpin1::En* mutants are based on null mutations and a complete loss of the *AtPIN1* expression, we conclude that the *pin-formed* and *Atpin1::En* mutants both lack the same component functional in polar auxin transport in *Arabidopsis* inflorescence axes (*13*).

The AtPIN1 protein. The predicted *AtPIN1* gene product is 622 amino acids long and includes 8 to 12 putative transmembrane segments flanking a central region that is predominantly hydrophilic (Fig. 2C). Similar topologies have been described for proteins that are involved in a wide variety of transmembrane transport processes (*14*). Database comparisons and screening of libraries with *AtPIN1* probes identified several *Arabidopsis* genes with similarity to *AtPIN1* (*15*). The homologous gene *AtPIN2* (also known as *EIR1*) may encode another catalytic subunit of auxin efflux carrier complexes that performs a similar function in root cells (*16*). Genes similar in sequence to the *AtPIN* genes were found in other plant species, even in the evolutionarily distant monocotyledonous species of maize and rice, indicating that *AtPIN1* and related genes may be of fundamental importance in plant development (*17*).

To analyze the function of the AtPIN1 protein in plants, we raised polyclonal antibodies to a portion (amino acid 155 to 408) of recombinant AtPIN1 with an NH_2-terminal His_6 affinity tag. The affinity-purified antibody to AtPIN1 (anti-AtPIN1) identified on protein immunoblots a protein from *Arabidopsis* microsomes matching the molecular

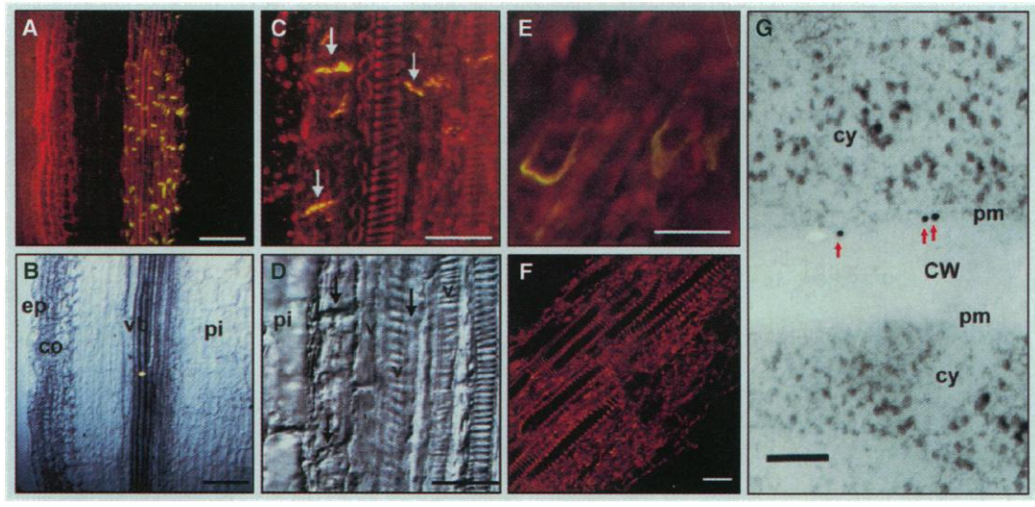

Fig. 4. AtPIN1 immunolocalization in longitudinal *Arabidopsis* tissue sections. (**A** to **F**) Indirect immunofluorescence analysis by laser scanning confocal microscopy. Stem segments of plants were fixed, sectioned, and incubated with polyclonal anti-AtPIN1 (*18*). Bound anti-AtPIN1 was indirectly visualized with the help of fluorescent (FITC) secondary antibodies (*30*). The immunofluorescent cells (green-yellow signals) formed continuous vertical cell strands in vascular bundles (A). The AtPIN1 signals are found at the basal end of elongated, parenchymatous xylem cells in the neighborhood of vessel elements, which are distinguished by secondary cell wall thickening structures (C). The red tissue autofluorescence [(A), (C), (E), and (F)] and comparison with the corresponding differential interference contrast (DIC) images [(B) and (D)] facilitated the histological localization of the AtPIN1-specific signals. The arrows point to the AtPIN1-specific fluorescence at the basal end of the xylem cells (C) or to the corresponding positions in the DIC image (D). They also indicate the direction of polar auxin transport in the tissue studied. In (C) two fluorescent signals of three cells forming a vertical cell strand are shown. The upper signal is found at the basal end of the cell extending out of the top of the picture. The cell underneath is fully shown in vertical extension, also fluorescently labeled at its basal end. The fluorescent signal of its basally contacting cell is not shown, because its basal end is out of the picture. A longitudinal hand section of an *Arabidopsis* stem is shown in (E). AtPIN1 immunofluorescence is primarily localized to the basal side of the cells extending slightly up the lateral walls. A control with a longitudinal section from the *Atpin1::En134* mutant is shown in (F). No AtPIN1-specific fluorescent signals were detected. (**G**) Ultrathin tissue sections were incubated with the polyclonal anti-AtPIN1 and gold-coupled secondary antibodies and examined with an electron microscope (*18*, *31*). Gold grains (marked by arrows) were detected only in one membrane of two contacting cells and were absent at the opposite plasma membrane. ep, epidermis; co, cortex; cw, cell wall; cy, cytoplasm; pm, plasma membrane; pi, pith; v, vessel; vb, vascular bundle. Size bars represent 25 μm [(C), (E), and (F)], 100 μm (A), and 0.1 μm (G).

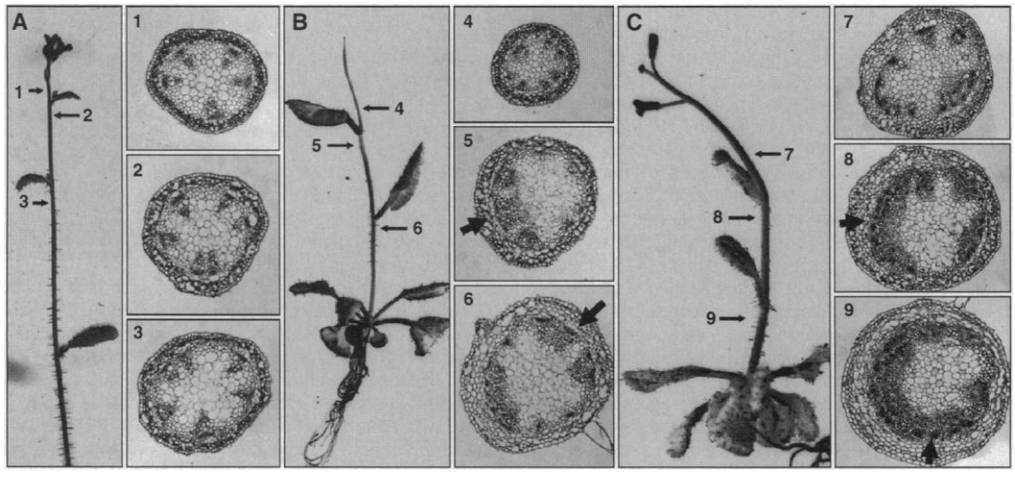

Fig. 5. Analysis of vascular patterning in *Atpin1::134* mutants (*32*). Inflorescence of a wild-type Columbia *Arabidopsis* plant (**A**), an *Atpin1::En134* mutant (**B**), and a wild-type plant (**C**), grown in the presence of auxin transport inhibitor NPA (15 μM). Cross sections were cut as indicated by arrows in (A), (B), (C). The sections presented were cut just above the first cauline leaf (1, 4, 7) and directly below the first (2, 5, 8) and second cauline leaves (3, 6, 9). Arrows on the cross sections (5, 6, 8, 9) indicate the position of the leaves above. Abnormal xylem proliferation was observed in the inflorescence axis below cauline leaves, adjacent to the leaf attachment site. The diameters of the stem sections are ~1 to 2 mm.

mass of 67 kD predicted for AtPIN1 (*18*).

Polar localization of AtPIN1. To localize the *AtPIN1* gene products in situ, we probed cross sections of *Arabidopsis* inflorescence axes with antisense *AtPIN1* RNA and polyclonal anti-AtPIN1. In both cases parenchymatous xylem and cambial cells were labeled (Fig. 3, C to G). Probing longitudinal sections from *Arabidopsis* inflorescence axes with affinity-purified anti-AtPIN1, we observed labeling at the basal end of elongated parenchymatous xylem cells (Fig. 4, A to E). The basal-apical orientation of the cells was identified with the help of angled razor cuts and residual leaf bases on the excised stem segments. AtPIN1-specific fluorescent signals were primarily located to the basal side of the plasma membrane, with some signal extending beyond the basal side forming a U-shaped fluorescent zone (Fig. 4E). Immunogold labeling and electron microscopy of longitudinal tissue sections revealed gold grains exclusively at the upper membrane of two contacting cells (Fig. 4G). The polar localization of AtPIN1 in these tissues is consistent with the proposed distribution of auxin efflux carriers that mediate shoot-basipetal auxin transport (*2*, *5*, *19*).

Alteration of vascular development. In intact plants, the polar flow of auxin is essential for the formation of spatially organized patterns of vascular tissues (*3*). We therefore tested whether genetic disruption of the *AtPIN1* gene affected vascular pattern formation. In cross sections below the first cauline leaf of *Atpin1::134* mutant inflorescence axes, we observed massive radial xylem proliferation in the vascular bundles adjacent to the cauline leaf (Fig. 5). Sections below the second cauline leaf confirmed extensive xylogenesis in the vascular bundles originating from the leaves above. The increase of vascular tissue at positions just below where young auxin-synthesizing leaves were connected to the axial vascular system is consistent with the view that poor basipetal transport in *Atpin1* mutants reduces the drainage of auxin from the leaves, leading to enhanced xylem proliferation in the vicinity. Chemical inhibition of polar auxin transport in wild-type plants caused very similar alterations in radial vascular pattern formation (Fig. 5). This indicates that the genetic defect in *Atpin1* mutants correlates with a defect of cellular auxin efflux at the site of the inhibitor 1–naphthylphthalamic acid (NPA) action in polar auxin transport (*2*, *20*). Enhanced vascular tissue differentiation has also been observed in plants that overproduce auxin, supporting a role of auxin gradients in radial vascular pattern formation (*21*). We suggest that both the mutations in the *AtPIN1* locus (*Atpin1:: En* and *pin-formed* mutants) as well as the chemical inhibition reduced auxin efflux and led to similar alterations in vascular development.

The reduction of polar auxin transport in *Atpin1* mutants and its effects on plant development indicate a role of AtPIN1 in polar auxin transport, most likely in supporting efflux of auxin from the cell. On the basis of the predicted topology of AtPIN1, its homology to carrier proteins, and its polar localization in auxin transport–competent cells, we propose that AtPIN1 might act as a catalytic auxin efflux carrier protein in basipetal auxin transport.

References and Notes

1. C. Darwin, *The Power of Movements in Plants* (John Murray, London, 1880); F. W. Went, *Rec. Trav. Bot. Neerl.* **25**, 1 (1928); G. H. van der Weij, *ibid.* **31**, 810 (1934).
2. M. H. M. Goldsmith, *Annu. Rev. Plant Physiol.* **28**, 439 (1977); T. L. Lomax, G. K. Muday, P. H. Rubery, in *Plant Hormones, Physiology, Biochemistry and Molecular Biology*, P. J. Davies, Ed. (Martinus Nijhoff, Kluwer, Dordrecht, The Netherlands, 1995), pp. 509–530.
3. T. Sachs, *Pattern Formation in Plant Tissues* (Cambridge Univ. Press, Cambridge, 1991); R. Aloni, in *Plant Hormones, Physiology, Biochemistry and Molecular Biology*, P. J. Davies, Ed. (Martinus Nijhoff, Kluwer, Dordrecht, The Netherlands, 1995), pp. 531–546.
4. M. Jacobs and P. H. Rubery, *Science* **241**, 346 (1988).
5. M. Jacobs and S. F. Gilbert, *ibid.* **220**, 1297 (1983).
6. K. Okada, J. Ueda, M. K. Komaki, C. J. Bell, Y. Shimura, *Plant Cell* **3**, 677 (1991).
7. S. R. M. Bennett, J. Alvarez, G. Bossinger, D. R. Smyth, *Plant J.* **8**, 505 (1995).
8. G. H. Cardon, M. Frey, H. Saedler, A. Gierl, *Plant J.* **3**, 773 (1993). The heterozygous *Atpin1::En134* mutant (M_1), whose M_2 progeny segregated 3:1 for wild-type and mutant phenotypes, was identified in generation S_6 [E. Wisman, G. H. Cardon, P. Fransz, H. Saedler, *Plant Mol. Biol.* **37**, 989 (1998)]. Backcrosses of heterozygous *Atpin1::En134* plants with wild type expressed the mutant phenotype only in the F_2 generation.
9. L. Gälweiler *et al.*, data not shown.
10. Crosses between the heterozygous transposon insertional mutants yielded ~25% mutant phenotypes in the F_1 generation, indicating allelism. Using *En-1*– and *AtPIN1*-specific primers, we amplified the transposon-flanking DNA in the *Atpin1::En111*, *Atpin1::En134*, and *Atpin1::En349* alleles by PCR and then sequenced it. The sequences were identical with *AtPIN1* sequences showing independent *En-1* insertions.
11. Plant DNA sequences flanking the 5′ end of *En-1* in the *Atpin1::En134* allele were cloned by a ligation-mediated PCR technique [P. R. Mueller and B. Wold, *Science* **246**, 780 (1989); M. Frey, C. Stettner, A. Gierl, *Plant J.* **13**, 717 (1998)] with *En-1*– and linker-specific oligonucleotides after Csp6 I restriction of genomic DNA and ligation of compatible linker DNA. The isolated flanking DNA was used as a probe to screen a cDNA library, prepared from suspension cells, for homologous clones that were then used to screen a genomic library of *A. thaliana*. The λ libraries were prepared from the ecotype Columbia and provided by the Arabidopsis DNA Centre, Cologne. Sequence analysis of the longest *AtPIN1* cDNA (2276 base pairs) identified an open reading frame encoding 622 amino acids. An in-frame stop codon located upstream to the first ATG suggested that the cDNA encodes a full-length protein. GenBank accession numbers are as follows: AF089084 (*AtPIN1* cDNA) and AF089085 (*AtPIN1* genomic DNA).
12. By screening the CIC YAC library {[F. Creusot *et al.*, *Plant J.* **8**, 763 (1995)]; provided by the Arabidopsis DNA Centre, Cologne} with a radiolabeled *AtPIN1* probe, we identified a contig consisting of the overlapping clones CIC6H1, CIC12G10, CIC12H9, and CIC9C4. Physical mapping was performed with the server http://cbil.humgen.upenn.edu/~atgc/physical-mapping.
13. Repeating auxin transport measurements with stem segments, we confirmed the reduction of polar auxin transport in *pin-formed* mutants (*6*, *7*) and found a reduction of polar auxin transport in *Atpin1::En134* mutants as well.
14. S. J. Singer, *Annu. Rev. Cell Biol.* **6**, 247 (1990); M. D. Marger und M. H. Saier Jr., *Trends Biochem. Sci.* **18**, 13 (1993); H. Logan, M. Basset, A.-A. Véry, H. Sentenac, *Physiol. Plant.* **100**, 1 (1997).
15. GenBank accession numbers of homologous clones in *Arabidopsis thaliana* are as follows: ACC002311, AF056026 (*EIR1*), AF086906 (*AtPIN2* cDNA), AF086907 (*AtPIN2* genomic DNA), AC002291, AC005560, AB017068, AC004260, ACC003979, AF087016, AF087818, AF087819, AF087820, B61585, T43636, T04468, Z38079, and R84151.
16. C. Luschnig, R. A. Gaxiola, P. Grisafi, G. F. Fink, *Genes Dev.* **12**, 2175 (1998); A. Müller *et al.*, *EMBO J.* **17**, 6903 (1998). *AtPIN2* (AF086906) and *EIR1* (AF056026) were independently isolated and represent the same genetic locus.
17. GenBank numbers of *AtPIN1* homologous rice clones are as follows: AF056027 (*REH*), D25054, C27713, and C26920.
18. To generate AtPIN1-specific polyclonal antibodies, we ligated a Rsa I fragment of the *AtPIN1* cDNA encoding the antigenic peptide of AtPIN1 from amino acid 155 to 408 into the bacterial expression vector pQE-31 (Qiagen). This expression construct encoded a recombinant fusion protein with an NH_2-terminal His_6 tag. After expression in *Escherichia coli* SG13009, the recombinant protein was affinity purified on a Ni^{2+}–nitrilotriacetic acid column as described by the Quiaexpressionist manual (Qiagen) and checked by SDS–polyacrylamide gel electrophoresis [U. K. Laemmli, *Nature* **227**, 680 (1970)]. After immunization of rabbits (Eurogentec, Ougrée, Belgium), the polyclonal antiserum was affinity purified against the recombinant AtPIN1 peptide [J. Gu, G. Stephenson, M. J. Iadarola, *Biotechnlques* **17**, 257 (1994)] and diluted to a final protein concentration of 0.22 mg/ml. In protein immunoblot analysis the affinity-purified anti-AtPIN1 detected specifically the recombinant AtPIN1 peptide in bacterial extracts as well as a 67-kD protein in microsomal membrane fractions from *A. thaliana* [R. Zettl, J. Schell, K. Palme, *Proc. Natl. Acad. Sci. U.S.A.* **91**, 689 (1994)].
19. D. A. Morris and A. G. Thomas, *J. Exp. Bot.* **29**, 147 (1978).
20. A. Delbarre, P. Muller, V. Imhoff, J. Guern, *Planta* **198**, 532 (1996).
21. H. J. Klee, R. B. Horsch, M. A. Hinchee, M. B. Hein, N. L. Hoffmann, *Genes Dev.* **1**, 86 (1987); C. Uggla, T. Moritz, G. Sandberg, B. Sundberg, *Proc. Natl. Acad. Sci. U.S.A.* **93**, 9282 (1996).
22. T. Teichmann *et al.*, *Eur. J. Biochem.* **247**, 826 (1997).
23. F. M. Ausubel *et al.*, *Current Protocols in Molecular Biology* (Green, Wiley, New York, 1993).
24. The 3′ *En-1* probe DNA was generated by PCR with the *En-1*–specific primers En 7631 (5′-TCAGGCTCA-CATCATGCTAGTCC-3′) and En 8141 (5′-GGAC-CGACGCTCTTATGTTAAAAG-3′). In Southern blot analysis, this PCR product hybridized to the 3′ ends of Xba I–digested *En-1* DNA, detecting fragments of 1.98-kb *En-1* DNA plus flanking plant DNA.
25. Z. Schwarz-Sommer, A. Gierl, H. Cuypers, P. A. Peterson, H. Saedler, *EMBO J.* **4**, 579 (1985).
26. Single-letter abbreviations for amino acid residues are as follows: A, Ala; C, Cys; D, Asp; E, Glu; F, Phe; G, Gly; H, His; I, Ile; K, Lys; L, Leu; M, Met; N, Asn; P, Pro; Q, Gln; R, Arg; S, Ser; T, Thr; V, Val; W, Trp; and Y, Tyr.
27. J. Kyte and R. F. Doolittle, *J. Mol. Biol.* **157**, 105 (1982).
28. P. Chomczynski and N. Sacchi, *Anal. Biochem.* **162**, 156 (1987). To check for equal RNA loading we rehybridized the Northern blots with ribosomal protein large subunit 4 (*RPL4*) and ubiquitin carrier (*UBC*) probes.
29. Segments of inflorescence axes of 3- to 4-week-old *A. thaliana* ecotype Columbia (grown in a greenhouse at 18° to 24°C, with 16 hours of light) were fixed, paraffin embedded, and analyzed by in situ hybridization as described (*22*), with the following modifications. To generate *AtPIN1*-specific RNA probes, we inserted the Bgl II–Hind III fragment of the *AtPIN1* cDNA (base pairs 602 to 1099) into the Bam HI–, Hind III–cleaved vector pBluescript SK- (Stratagene),

generating pin23HX. After linearizing pin23HX (Hind III for antisense and Xba I for sense transcription), we performed in vitro transcription and digoxigenin labeling using the DIG RNA Labeling Kit (Boehringer Mannheim). The RNA hybridization was performed overnight at 42°C with a probe concentration of 30 ng per 100 μl. The slides were then washed with 4× standard saline citrate (SSC) containing 5 mM dithiothreitol (DTT) (10 min, room temperature), 2× SSC containing 5 mM DTT (30 min, room temperature), and 0.2× SSC containing 5 mM DTT (30 min, 65°C). After blocking with 0.5% blocking agent (Boehringer Mannheim), we detected signals using anti-digoxigenin (1:3000, Boehringer Mannheim) coupled to alkaline phosphatase followed by a nitroblue tetrazolium, brome-chloro-indolyl phosphate staining reaction.

30. Inflorescence axes of 3- to 4-week-old *Arabidopsis* wild-type and mutant plants (grown in a greenhouse at 18° to 24°C, with 16 hours of light) were cut and fixed in ice-cold methanol/acetic acid (3:1). Paraffin embedding, sectioning, and mounting were done as described (*22*). Antibody incubation and immunohistochemical staining was performed as described [S. Reinold and K. Hahlbrock, *Plant Physiol.* **112**, 131 (1996)], with the following modifications: 8-μm cross sections and 30-μm longitudinal sections of inflorescence axes were incubated with affinity-purified anti-AtPIN1 [(*18*), 4°C, overnight], diluted 1:100 in buffer [3% (w/v) milk powder in phosphate-buffered saline (PBS), pH 7.4]. Incubation with secondary antibodies coupled to fluorescein isothiocyanate (FITC) or alkaline phosphatase (Boehringer Mannheim, 1:100) was done at room temperature for 2 to 3 hours. After antibody incubation, washing was performed three times (10 min) with PBS containing 0.2% Tween 20. For hand sectioning, stem segments were fixed in 4% paraformaldehyde, diluted in MTSB (50 mM piperazine ethanesulfonic acid, 5 mM ethylene glycol tetraacetic acid, 5 mM $MgSO_4$, pH 7.0), treated with 2% Driselase (Sigma, in MTSB, 0.5 hour), and permeabilized with 10% dimethylsulfoxide and 0.5% NP-40 (in MTSB, 1 hour). After hand sectioning with razor blades, antibody incubation was performed as described above. Alkaline phosphatase staining reactions were carried out for several hours to overnight, and the results were analyzed microscopically. Fluorescent signal analysis was performed with a confocal laser scanning microscope (Leica DMIRBE, TCS 4D with digital image processing) with a 530 ± 15 nm band-pass filter for FITC-specific detection and a 580 ± 15 nm band-pass filter for autofluorescence detection. For histological signal localization both images were electronically overlaid, resulting in red autofluorescence and green-yellow AtPIN1-specific fluorescence. DIC images were generated to determine the exact cellular signal localization. Controls with preimmune serum and secondary antibodies alone yielded no specific signals. Tissue orientation of the longitudinal stem sections was determined with the help of residual traces of lateral leaves and by cutting stem segments apically and basally with different angles. Polar signal localization was also obvious in cells in which the immunostained cytoplasm was detached from the basal cell wall (*9*). The AtPIN1 localization results were reproduced by several experiments.

31. Tissue was frozen with an HPM 010 high-pressure instrument (Balzers, Liechtenstein) and processed as described [K. Mendgen, K. Welter, F. Scheffold, G. Knauf-Beiter, in *Electron Microscopy of Plant Pathogens*, K. Mendgen and K. Lesemann, Eds. (Springer-Verlag, Heidelberg, 1991), pp. 31–42]. Substitution was performed in acetone at –90°C, embedding in Unicryl (British Biocell, Cardiff), and polymerization at 4°C. Ultrathin sections were incubated with primary antibodies [1% preimmune serum or affinity-purified anti-AtPIN1 (*18*)], diluted 1:10 with buffer [1% (w/v) bovine serum albumin (BSA) and 0.1% BSA-C, in TBS (10 mM tris(hydroxymethyl)aminomethane-HCl, 150 mM NaCl, pH 7.4)], for 3 hours, followed by incubation with a secondary antibody [10 nm gold coupled to goat antibody to rabbit immunoglobulin G (Biotrend, Köln, Germany)], diluted 1:20 with buffer, for 1 hour at 20°C. Sections were stained with uranylate and lead citrate and examined with an Hitachi H-7000 electron microscope.
32. Plants were grown in vitro as described (*6*), fixed, paraffin-embedded, and deparaffinated as described (*22*). Cross sections (10 μm) of inflorescence axes were analyzed microscopically. Anatomical studies with *pin-formed* plants gave similar results.
33. We thank P. Huijser for help with the confocal microscopic analysis, H. Vahlenkamp for electron microscopy, C. Koncz for comments on the manuscript, and H. Saedler and J. Schell for continuous support and help. Funded by the European Communities' BIOTECH program and by the Deutsche Forschungsgemeinschaft "*Arabidopsis*" program.

23 September 1998; accepted 11 November 1998

A Free-Fall Determination of the Newtonian Constant of Gravity

Joshua P. Schwarz, Douglas S. Robertson, Timothy M. Niebauer, James E. Faller

Recent determinations of the Newtonian constant of gravity have produced values that differ by nearly 40 times their individual error estimates (more than 0.5%). In an attempt to help resolve this situation, an experiment that uses the gravity field of a one-half metric ton source mass to perturb the trajectory of a free-falling mass and laser interferometry to track the falling object was performed. This experiment does not suspend the test mass from a support system. It is therefore free of many systematic errors associated with supports. The measured value was $G = (6.6873 \pm 0.0094) \times 10^{-11}$ m^3 kg^{-1} sec^{-2}.

Here we report a method for determining the Newtonian gravitational constant, G, by measuring the perturbation to the acceleration of a free-falling object due to a well-known source mass. A precise knowledge of G is of considerable metrological interest, for it provides a unique as well as valuable measurement challenge that sharpens and prepares experimental skills to better deal with a variety of precision and null experiments. Yet despite two centuries of experimental effort, the value of G remains poorly known; recent determinations of G differ by as much as 40 times their individual estimates of uncertainty, suggesting the presence of significant systematic errors. The difficulty in measuring G stems in part from the extreme weakness of the gravitational force and the consequent difficulty of generating a sufficiently large signal for accurate measurement. Additional problems arise from the difficulty of eliminating spurious forces because of such things as electromagnetic fields and thermal gradients.

In 1798 Henry Cavendish performed the first experiment specifically designed to investigate the gravitational attraction between small masses using a torsion balance to match the tiny gravitational force produced by local source masses against the restoring torque of a fiber support. This was the first laboratory measurement of this elusive fundamental constant. In the 1930s Heyl reintroduced the "time-of-swing" measurement, in which source masses modulate the oscillation frequency of a torsion pendulum. Both types of torsion methods introduce experimental difficulties that center on the need to calibrate precisely the restoring force. Indeed, the subtle properties of torsion fibers are still being investigated (*1–3*).

In 1982 Luther and Towler (*4*) used the time-of-swing method to achieve a value of G that because of its small error is the dominant contributor to the value that is accepted today. More recently, Fitzgerald and Armstrong (*5*) developed a compensated torsion balance in which electrostatic forces cancel out the gravitational force of the source masses, and Michaelis and co-authors (*6*) experimented with a compensated torsion balance using a fluid mercury bearing instead of a fiber as a support. Walesch, Meyer, Piel, and Schurr (*7,8*) introduced a dual pendulum method in which the gravitational gradient of a source mass is measured through its effect on the length of a Fabry-Pérot cavity supported by two pendulums at different distances from the mass. Finally, Schurr, Nolting, and Kündig (*9*) recently published the experimental results obtained using a beam-balance method [see (*10*) for discussion of these and other experiments].

The values for G determined from these experiments differ by more than 40 times the quoted standard errors. This situation—dis-

J. P. Schwarz and J. E. Faller, JILA, University of Colorado and National Institute of Standards and Technology, Boulder, CO 80309–0440, USA. D. S. Robertson, National Geodetic Survey, NOS, NOAA, and CIRES, University of Colorado, Boulder, CO 80309–0216, USA. T. M. Niebauer, Department of Geophysics, Colorado School of Mines, Golden, CO 80401, USA.